Organic Geochemistry 108 (2017) 18–29

Contents lists available at ScienceDirect

Organic Geochemistry

journal homepage: www.elsevier.com/locate/orggeochem

Origin, charging, and mixing of crude oils in the Tahe oilfield, Tarim Basin, China

Zhao-Wen Zhan, Yan-Rong Zou *, Changchun Pan, Jia-Nan Sun, Xiao-Hui Lin, Ping'an Peng

State Key Laboratory of Organic Geochemistry, Guangzhou Institute of Geochemistry, Chinese Academy of Sciences, Guangzhou, 510640, China

ARTICLE INFO

Article history:
Received 24 September 2016
Received in revised form 9 March 2017
Accepted 16 March 2017
Available online 3 April 2017

Keywords:
Mixed oil
De-convoluting
Alternating least squares
Oil charging pathway
Tarim Basin

ABSTRACT

Forty-eight crude oil samples collected from different reservoirs in the Tahe oilfield of the Tarim Basin were investigated. Based on geochemical characteristics, it is concluded that the oil samples originated from multiple marine source rocks deposited in various sedimentary environments and subsequently altered by different levels of thermal maturation. These mixtures were de-convoluted to three endmember oils (EM1, EM2 and EM3) by alternating least squares regression using 38 concentration parameters. EM1 is the minimum contributor with an average of 13%, while EM2 and EM3 are the main contributors to the mixtures with averages of 52% and 35%, respectively. EM1 oil originated from Cambrian–Lower Ordovician source rocks in the early to peak oil window and subsequently experienced two phases of mixing and biodegradation. EM2 and EM3 oils originated from Middle–Upper Ordovician source rocks, but EM2 was generated at lower thermal maturity than EM3. The EM2 oil underwent two phases of mixing and one stage biodegradation, while the EM3 oil mixed with previous existing mixtures in the reservoirs. The final mixtures that might be affected by secondary processes, such as evaporative fractionation, are currently produced from the Tahe oilfield. The general orientation of oil filling was from south to north and east to west based on variations in the relative contributions of EMs, and the total concentrations of dibenzothiophenes and dibenzofurans in the oils. Considering the histories of sedimentary tectonic evolution, hydrocarbon generation and expulsion, and the de-convolution results, a model of three stages of oil charge and two phases of mixing and biodegradation was established for the Tahe oilfield oils.

1. Introduction

The Tahe oilfield is characterized by the coexistence of various types of fluids including waxy, heavy, and normal oils, and condensate. Like other marine oils in the Tarim Basin, the origin and accumulation mechanisms for oils in the Tahe oilfield are still hotly disputed. An increasing number of studies suggest that marine oils in the Tabei Uplift (including the Tahe oilfield) are mixtures generated from two marine source rocks, Cambrian–Lower Ordovician (ϵ-O_1) and Middle–Upper Ordovician (O_{2-3}) strata, or different hydrocarbon generation stages (Tao et al., 2010; Yu et al., 2011, 2012; Tian et al., 2012a; Zhu et al., 2013; Li et al., 2015a). Multiple tectonic movements and multiple generation, migration, accumulation, and secondary alteration processes, including thermal cracking, biodegradation and fractionation, are generally presumed to have caused physicochemical changes that made oil compositions extremely complex (Zhang and Huang, 2005; Zhang et al., 2005, 2014; Li et al., 2010a).

There are two key points that contribute to ambiguous results when deconvoluting the mixtures. First, inconsistent conclusions are drawn from different parameters for oil-source rock correlation. For example, the sterane biomarker distributions in the Tabei marine oils show a genetic relationship with the O_{2-3} source rocks (Ma et al., 2004; Zhang and Huang, 2005), whereas distributions of aryl isoprenoids are more closely correlated to ϵ-O_1 source rocks (Sun et al., 2003), and carbon isotopic compositions suggest that mixed source facies contributed to the crudes (Li et al., 2010b, 2015b; Jia et al., 2013). Second, correct identification of endmembers is a key to the quantitative evaluation of mixed oils, because incorrect assumptions of endmember compositions can lead to erroneous mixing models. For example, based on individual *n*-alkane isotopic values, the proportion of the ϵ–O_1-derived oils in the Tarim Basin ranged of 19–100% when the YG2 oil was used as the endmember to represent an O_{2-3} origin (Li et al., 2015b). However, a lower proportion ranging from 13–91% was obtained if the YM2 endmember oil is applied (Li et al., 2010b). Purely based

* Corresponding author. Fax: +86 20 85290706.
E-mail address: zouyr@gig.ac.cn (Y.-R. Zou).

http://dx.doi.org/10.1016/j.orggeochem.2017.03.007
0146-6380/

on bulk carbon isotopic variations between the two endmembers, the TZ62 Silurian oil and YM2 Ordovician oil represent ϵ-O_1 and O_{2-3} origins, respectively. Tian et al. (2012b) calculated the percentages of the ϵ-O_1 source contribution ranging between 10% and 100% for oils from Tazhong Uplift. Thus, endmember selection has a significant impact on interpretations. If the end-member selection is unreliable, all of these correlations and quantification estimates are misleading (Huang et al., 2016).

In our previous paper, we used a chemometric method that can simultaneously process almost all parameters and infer endmembers without a priori knowledge of the compositions of those endmembers to de-convolute the crude oils from Palaeozoic reservoirs in the Tabei Uplift, Tarim Basin (Zhan et al., 2016a). In the present study, forty-eight different crude oil samples from the Tahe oilfield located at the Akekle High, a small secondary structure of the Tabei Uplift, are selected to determine the number of endmember oils, the relative contributions of each endmember, and discuss the regional filling direction of oil entering the reservoirs. The aim is a better understanding of reservoir filling and oil mixing histories. This paper is building on our previous work (Zhan et al., 2016a,b) and is a practical application of chemometrics in reservoir geochemistry.

2. Geological setting

The Tahe oilfield on the south slope of Akekule High in the Tabei Uplift is bounded by the Canhu Depression to the east, the Halahatang Depression to the west, and the Shuntuoguole Uplift and the Manjiaer Depression to the south (Fig. 1). The Akekule High is a long-term structural high developed on pre-Sinian metamorphic basement, which underwent multi-stage tectonic movements and deformation. It experienced three periods of tectonic evolution including: (1) Late Caledonian-Early Hercynian uplift and regional sedimentary discontinuity resulting in the formation of a paleo-morphological high and hiatus in the Silurian, Devonian and even part of the Middle-Upper Ordovician. (2) Later Hercynian compressional uplift, in which sedimentation ceased and denudation occurred once again. During this stage, severe structural deformation occurred in the south slope and main part of the morphological high, forming a series of anticlines and faults with near east-to-west orientation. (3) During the Yanshan-Himalaya, the paleo-morphological high subsided and received continental deposits. During the later Himalayan deformation, structural features of the Akekule High were transformed from north-to-south in the early to the present-day south-to-north orientation. During the basin evolution, sustained tectonic activity and multi-phase superposition of faults formed the present-day complex fault system, which controlled the multi-stage hydrocarbon accumulation and a complex reservoir distribution in this region.

The Tahe oilfield comprises multi-layered oil pays in Ordovician, Carboniferous, and Triassic reservoirs. The main reservoirs are Ordovician carbonates (karst reservoirs) in the Yingshan ($O_{1-2}y$) and Yijianfang (O_2yj) formations. The Carboniferous and Triassic reservoirs are clastic strata, including the Kalashayi (C_1kl, sandstone and interbedded mudstone), Akekule (T_2a, sandstone) and Halahatang (T_3h, sandstone) formations, and occur mainly in the eastern part of the Tahe Oilfield. There are many trap configurations in the Tahe oilfield, including structural, stratigraphic, and composite traps. The stratigraphic traps are mainly controlled by unconformities, lithofacies changes and sand body pinch-outs.

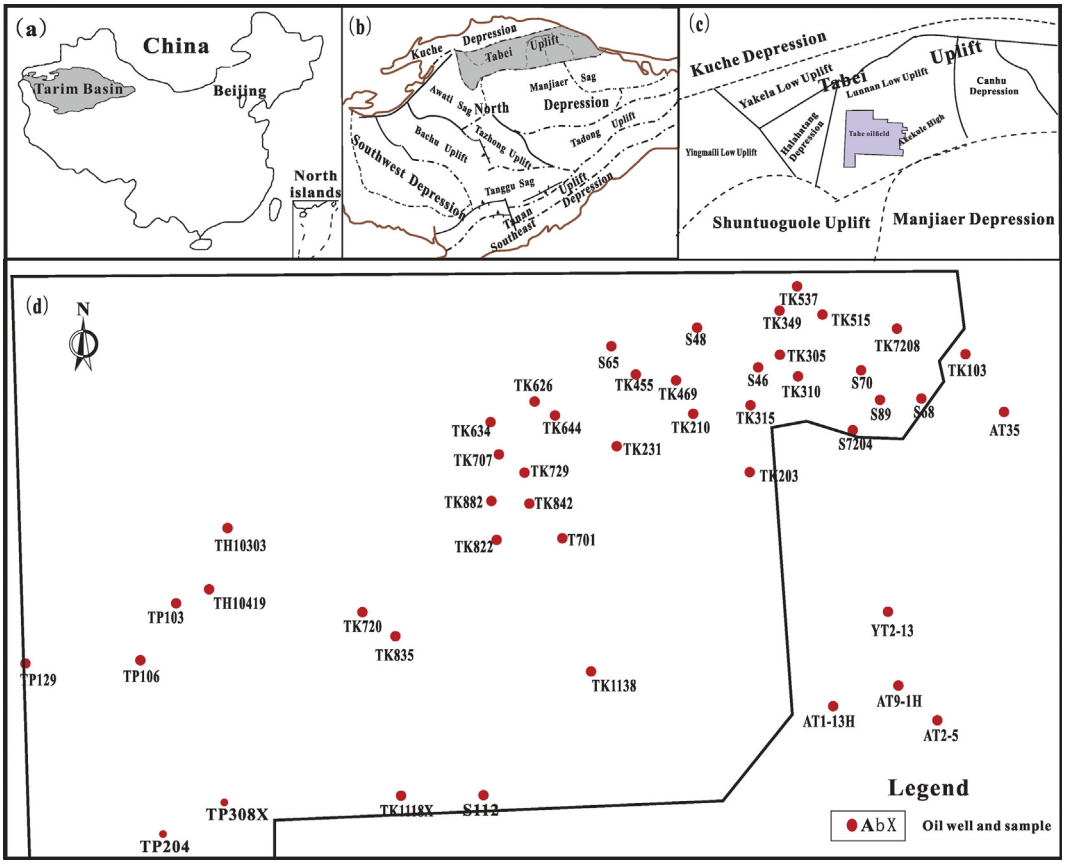

Fig. 1. Study area and sample locations. (a) Location of the Tarim Basin in China, (b) structural units in the basin, (c) location of the Tahe oilfield and (d) oil wells and sample distributions.

Table 1
Basic information of the samples and geochemical parameters discussed in the study.

Sample	Well	Reservoir	Depth/m	Density g/cm^3	δ^{13}Coil/‰	δ^{13}Csat./‰	δ^{13}Caro./‰	$\sum n$C/mg/g	$\sum n$C$_{21-}$/$\sum n$C$_{22+}$	R1	R2	R3	R4	R5	R6	R7	R8	R9	R10
1	AT2-5	T	4029–4033	0.87	/	−32.1	−31.6	111.09	3.55	0.28	0.33	0.88	0.86	0.21	0.04	0.43	0.49	0.63	0.12
2	AT1-13H	T	/	0.85	−32.6	−32.2	−32.2	128.20	5.44	0.30	0.37	0.87	0.96	0.32	0.08	0.37	0.50	0.64	0.09
3	AT9-1H	T	4608–4718	0.79	/	/	/	/	/	/	/	1.04	0.68	0.14	0.09	0.52	0.48	0.63	0.16
4	YT2-13	T	/	0.85	−32.5	−32.2	−32.1	107.43	4.48	0.30	0.36	0.90	0.85	0.33	0.09	0.35	0.49	0.63	0.09
5	TK203	T	4593–4597	0.83	−32.4	−32.3	−31.7	176.00	6.20	0.29	0.36	0.87	0.86	0.10	0.07	0.48	0.49	0.65	0.17
6	TK7208	T	4412–4415	0.84	−32.5	−32.4	−31.7	182.07	7.92	0.30	0.38	0.84	0.74	0.19	0.08	0.42	0.47	0.63	0.13
7	TK103	T	4514–4576	0.90	−32.7	−32.2	−32.3	65.60	4.74	0.32	0.37	0.90	1.13	0.20	0.07	0.34	0.51	0.64	0.08
8	TK305	C	5231–5239	0.84	−32.4	−32.3	−31.6	146.48	6.64	0.36	0.44	0.86	0.55	0.17	0.02	0.41	0.51	0.64	0.22
9	S70	C	5153–5168	0.83	/	−32.3	−31.7	130.26	4.03	0.33	0.39	0.82	0.89	0.22	0.06	0.41	0.47	0.63	0.23
10	TK310	C	5016–5019	0.82	−32.5	−32.5	−31.6	178.88	5.68	0.33	0.39	0.89	0.48	0.27	0.06	0.39	0.50	0.67	0.24
11	S89	O	5519–5550	0.86	−32.2	−31.8	−31.5	141.55	2.38	0.30	0.30	0.72	0.54	0.39	0.00	0.41	0.48	0.65	0.37
12	S68	O	/	0.82	−32.3	−32.2	−31.6	169.26	5.44	0.32	0.36	0.77	0.77	0.36	0.03	0.41	0.50	0.65	0.37
13	S7204	O	5783–6124	0.83	−32.8	−32.5	−31.7	173.54	5.75	0.37	0.50	0.86	0.93	0.28	0.00	0.32	0.49	0.63	0.22
14	AT35	O	5737–5855	0.85	−32.4	−32.3	−31.8	126.18	6.75	0.34	0.38	0.98	0.62	0.10	0.45	0.41	0.52	0.66	0.13
15	TK515	O	5471–5520	0.86	−32.4	−32.2	−31.9	131.59	6.82	0.35	0.39	0.97	0.60	0.27	0.35	0.37	0.53	0.64	0.14
16	TK515	O	/	0.86	−32.4	−32.0	−31.9	131.46	6.77	0.34	0.37	1.00	0.72	0.28	0.45	0.37	0.55	0.65	0.15
17	TP204	O	6348–6410	0.83	−32.6	−32.5	−31.7	130.34	4.52	0.39	0.48	0.79	0.64	0.17	0.00	0.42	0.50	0.66	0.40
18	TK1118X	O	6231–6249	0.83	/	−32.4	−31.4	98.34	3.53	0.34	0.40	0.91	0.41	0.51	0.09	0.55	0.52	0.66	0.62
19	TP308X	O	6584–6679	0.84	−32.8	−32.4	−31.6	170.19	5.94	0.33	0.40	0.80	0.42	0.09	0.00	0.39	0.49	0.66	0.45
20	S112	O	6172–6189	0.83	/	−32.6	−31.4	116.42	4.06	0.34	0.40	0.90	1.19	0.59	0.09	0.51	0.50	0.67	0.70
21	TK1138	O	5936–6019	0.84	−32.4	−31.9	−31.5	156.72	6.30	0.31	0.37	0.75	0.71	0.19	0.01	0.41	0.49	0.64	0.21
22	TK720	O	6120–6231	0.91	−32.9	−32.5	−32.4	95.08	6.24	0.36	0.44	0.96	0.97	0.30	0.08	0.36	0.48	0.64	0.09
23	TK835	O	5765–5840	0.93	/	−32.7	−32.3	49.05	3.30	0.35	0.44	0.96	1.07	0.19	0.05	0.35	0.49	0.64	0.08
24	TP129	O	6614–6682	0.91	−32.5	−32.3	−32.0	35.28	5.15	0.58	0.65	0.99	0.98	0.32	0.32	0.40	0.53	0.64	0.37
25	TH10419	O	6068–6148	0.92	−32.6	−32.3	−32.4	24.51	4.97	0.42	0.55	0.94	0.81	0.29	0.09	0.33	0.52	0.64	0.17
26	TP103	O	6130–6218	0.91	−32.9	−32.6	−32.2	68.37	4.32	0.43	0.55	0.95	0.89	0.24	0.11	0.32	0.49	0.63	0.18
27	TP106	O	6299–6365	0.93	/	−32.8	−32.1	28.19	2.43	0.45	0.62	0.96	0.95	0.21	0.15	0.33	0.50	0.62	0.17
28	TH10303	O	6084–6179	0.95	−32.8	−32.6	−32.2	45.20	6.12	0.42	0.50	1.05	1.04	0.25	0.18	0.30	0.50	0.63	0.13
29	T701	O	/	0.84	−32.7	−32.6	−31.1	156.29	5.53	0.35	0.46	0.79	0.77	0.17	0.02	0.33	0.50	0.65	0.19
30	TK707	O	5708–5767	0.98	/	−32.5	−32.4	14.76	3.24	0.47	0.66	0.97	0.99	0.15	0.04	0.35	0.49	0.64	0.10
31	S46	O	5373–5455	0.96	/	−32.4	−32.2	56.73	3.60	0.36	0.45	0.91	0.75	0.14	0.08	0.30	0.50	0.64	0.11
32	TK882	O	5727–5765	0.87	−32.9	−32.6	−32.5	62.39	6.47	0.36	0.44	0.99	1.16	0.21	0.07	0.34	0.49	0.62	0.08
33	TK842	O	5528–5620	0.93	/	−32.7	−32.7	26.54	2.90	0.37	0.47	0.99	1.22	0.15	0.10	0.32	0.50	0.64	0.07
34	TK349	O	5373–5428	0.87	−32.9	−32.5	−32.4	119.48	5.76	0.35	0.47	0.95	1.02	0.14	0.10	0.29	0.51	0.65	0.08
35	TK231	O	5550–5585	0.92	−32.6	−31.8	−32.5	21.91	5.97	0.36	0.45	0.96	1.11	0.20	0.10	0.33	0.50	0.63	0.07
36	TK315	O	5431–5498	0.94	/	−32.7	−32.6	35.38	2.72	0.37	0.50	0.97	1.06	0.21	0.10	0.28	0.49	0.62	0.07
37	TK729	O	/	0.97	−32.9	−32.4	−32.6	28.84	6.08	0.36	0.47	1.00	1.08	0.27	0.12	0.33	0.50	0.63	0.07
38	TK822	O	5631–5632	0.95	−32.9	−32.5	−32.7	53.75	5.85	0.36	0.46	1.03	1.18	0.30	0.11	0.32	0.49	0.62	0.07
39	TK537	O	5387–5452	0.92	−33.2	−32.7	−32.7	51.80	4.89	0.38	0.50	0.98	1.10	0.22	0.13	0.31	0.50	0.64	0.07
40	S48	O	5363–5370	0.96	/	−32.4	−32.5	20.96	4.24	0.38	0.51	1.00	1.09	0.20	0.14	0.34	0.52	0.65	0.07
41	TK644	O	5565–5607	0.96	/	−32.7	−32.5	18.54	3.34	0.36	0.47	1.02	1.20	0.22	0.17	0.32	0.50	0.64	0.07
42	TK210	O	5448–5560	0.98	/	−32.4	−32.7	27.58	3.65	0.38	0.47	1.01	1.24	0.22	0.16	0.32	0.51	0.63	0.07
43	TK626	O	/	0.97	−33.1	−32.4	−32.7	39.76	6.24	0.35	0.48	1.05	1.25	0.21	0.15	0.31	0.49	0.63	0.06
44	TK634	O	5567–5599	0.97	/	−32.6	−32.7	19.67	3.56	0.37	0.49	1.03	1.22	0.22	0.17	0.32	0.50	0.64	0.06
45	TK469	O	5562–5620	0.97	/	−32.6	−32.6	23.83	3.66	0.37	0.48	1.04	1.15	0.22	0.18	0.33	0.48	0.63	0.07
46	TK469	O	5548–5560	0.95	/	−32.6	−32.7	23.56	3.04	0.37	0.48	1.06	1.10	0.23	0.18	0.32	0.48	0.63	0.07
47	TK455	O	5482–5548	0.97	/	−32.6	−32.8	24.35	4.51	0.37	0.48	1.03	1.20	0.23	0.18	0.32	0.51	0.64	0.06
48	S65	O	5451–5585	0.97	−33.0	−32.6	−32.8	37.25	5.97	0.37	0.48	1.08	1.21	0.11	0.19	0.33	0.52	0.65	0.06

Note: O, Ordovician; C, Carboniferous; T, Triassic. Sat., saturate; Aro., aromatic; $\sum n$C$_{21-}$, $\sum n$C$_{22+}$, the sum of low, high molecular-weight *n*-alkanes, respectively; $\sum n$C, total *n*-alkane concentration; R1 = Pristane/C$_{17}$-alkane; R2 = Phytane/C$_{18}$-alkane; R3 = C$_{29}$H/C$_{30}$H, [T14/T15]; R4 = C$_{35}$H/C$_{34}$H, [T21/T20]; R5 = G/C$_{30}$H, [T17/T15]; R6 = 25N-C$_{29}$H/C$_{30}$H, [T23/T15]; R7 = diaC$_{27}$/regC$_{27}$ steranes, [T3/(sum of S4 to S7)]; R8 = sterane C$_{29}\alpha\alpha\alpha$20S/(20S + 20R), [S12/(S12 + S15)]; R9 = sterane C$_{29}\beta\beta$/($\alpha\alpha$ + $\beta\beta$), [(S13 + S14)/(sum of S12 to S15)]; R10 = TAS(I)/TAS(I + II) = (C$_{20}$ + C$_{21}$ triaromatic pregnanes)/(C$_{26}$20S + C$_{26}$20R + C$_{27}$20S + C$_{28}$20S + C$_{27}$20R + C$_{28}$20R triaromatic steranes). The symbols for the biomarkers are described in notes to Tables 2 and 3; /, no data or no detection.

3. Samples and methods

3.1. Samples

A total of 48 crude oil samples collected from the Tahe oilfield were investigated in this study. They were recovered from different depths and reservoirs (Table 1) and stored in a refrigerator. Thirty-eight samples are from Ordovician, three are from Carboniferous, and seven are from Triassic reservoirs. Their locations are shown in Fig. 1.

3.2. Experimental analysis

A certain volume of CS_2 (1–2 mL) was added to the measured oil sample with the internal standard n-$C_{24}D_{50}$ of known concentration. The mixture was allowed to stand for more than one night (> 12 h) and the supernatant was analyzed using a SHIMADZU GC-2010Plus equipped with a flame ionization detector (FID). A PONA capillary column (50 m, 0.20 mm i.d., and 0.50 μm film thickness) was used with helium as the carrier gas (constant flow, current speed 1.0 mL/min). The initial GC oven temperature was 30 °C, which was held isothermal for 10 min, then programmed to 90 °C at 3 °C/min, finally it was raised to 300 °C at a rate of 4 °C/min, and then held isothermal for 45 min.

The experimental methods and analysis conditions of oil fractionation, gas chromatography mass spectrometry (GCMS), and Carbon isotopic analysis of bulk oil and fractions were described by Zhan et al. (2016b).

3.3. Alternating least squares (ALS) de-convoluting

Chemometrics uses multivariate statistics to recognize patterns and extract useful information from measured data (Peters et al., 2005). Some successful applications in petroleum geochemistry have been previously reported (Peters et al., 2007, 2013, 2016). The principles and applications of ALS to de-convolute mixed oils were discussed in detail by Peters et al. (2008) and Zhan et al. (2016a,b). In the present study, ALS from Pirouette® software version 4.5 (Infometrix, Inc.) was employed to de-convolute mixed oils from the Tahe oilfield in the Tarim Basin. In ALS, rows were chosen to produce the initial estimates. Some constraints include non-negativity of amounts and profiles and closure of amounts.

4. Results and discussion

4.1. Geochemical characteristics of the oils

The oil samples in our study from the Tahe oilfield have widely variable bulk characteristics. The densities of these oils range from 0.79 g/cm^3 to 0.98 g/cm^3 (Table 1), showing systematic variations along the transect from south to north (discussed in Section 4.2.3). Bulk compositions vary significantly, whereas stable carbon isotope ratios ($\delta^{13}C$) show relatively small variations (Table 1). The whole oil $\delta^{13}C$ of the samples ranges from −33.2‰ to −32.2‰, with an average of −32.7‰. The saturate and aromatic hydrocarbons $\delta^{13}C$ of these oils range from −32.8‰ to −31.8‰ and −32.8‰ to −31.1‰, with averages of −32.4‰ and −32.1‰, respectively. These values indicate all the oils as being sourced from similar marine source rocks, with subtle variations due to slight differences in maturity and/or organic facies (Sofer, 1984; Peters et al., 2005).

The n-alkane envelopes show maxima in the range of n-C_7 to n-C_{19}, and for most samples this occurs at carbon numbers less than n-C_{10}. The total n-alkane concentrations ($\sum n$-C) range from 14.8 mg/g to 182.1 mg/g oil and the abundance ratios of low to high molecular-weight n-alkanes ($\sum n$-C_{21-}/$\sum n$-C_{22+}) range from 2.38 to 7.92, suggesting high thermal maturity. Despite the large variability, there is a good positive relationship between Pr/n-C_{17} and Ph/n-C_{18} suggesting an origin dominated by algal kerogen (Connan and Cassau, 1980).

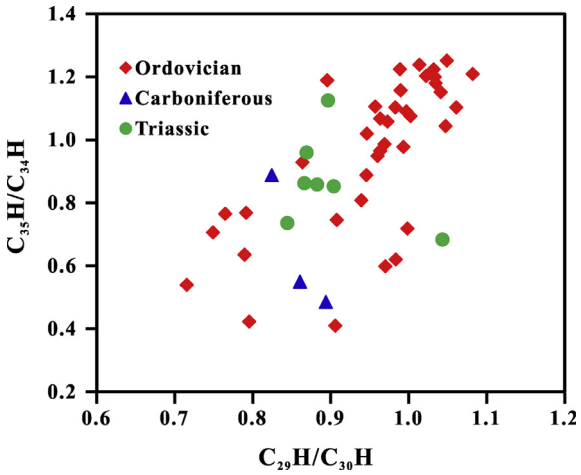

Fig. 2. Correlations of ratios of $C_{29}H/C_{30}H$ vs. $C_{35}H/C_{34}H$ of the oils.

The oils all have relatively high concentrations and presence of a complete series of tricyclic terpanes (C_{19}TT to C_{29}TT, without C_{27}TT). The relative abundance of the hopane series (H) varies greatly. Some samples are dominated by $C_{30}H$ with the relative intensities of homohopanes ($C_{31}H$-$C_{35}H$) decreasing with increasing carbon number, while other samples have the main hopane peak at $C_{29}H$ and more $C_{35}H$ than $C_{34}H$. High C_{35}/C_{34} homohopanes ($C_{35}H/C_{34}H$) indicate an anoxic depositional environment and High 30-norhopane/hopane ($C_{29}H/C_{30}H$) ratios are typical of anoxic carbonate or marl source rocks and related oils, but are also affected by thermal maturity (Peters et al., 2005). For the investigated samples, the ratios of $C_{29}H/C_{30}H$ and $C_{35}H/C_{34}H$ range from 0.72 to 1.08 and 0.41 to 1.25 (Table 1), respectively. The cross plot of these parameters show poor correlations (Fig. 2), indicating that they are derived from different marine sedimentary facies or organic facies source rocks.

The abundance of gammacerane as well as the content of C_{28} sterane is one of the main distinguishing features between ϵ-O_1 and O_{2-3} source rocks in the Tarim Basin. These parameters are enriched in the ϵ-O_1 rocks, while relatively low in the O_{2-3} rocks (Zhang et al., 2000, 2004, 2005; Ma et al., 2004). The Tahe oilfield oils have gammacerane indices ($G/C_{30}H$) ranging from 0.09 to 0.59 (Table 1). Concentrations of G and C_{28}-ααα 20R sterane vary from 5 to 228 ppm and 3 to 79 ppm (Tables 2 and 3), respectively. They also exhibit a good positive relationship in the oil samples (Fig. 3), suggesting that their contents increase with the progressively greater contribution from ϵ-O_1 source rocks.

The C_{29} steranes 20S/(S + R) and ββ/(ββ + αα) ratios are within the ranges of 0.47–0.55 and 0.62–0.67 in the investigated oils (Table 1) and approach or have reached to their respective equilibrium endpoints (0.52–0.55 and 0.67–0.71, respectively, Peters et al., 2005), indicating the oils were generated in the early to peak oil window. The ratio of diasteranes/steranes (dia/reg) and the triaromatic steroids ratio [TA(I)/TA(I + II)] are proposed as maturity parameters for crude oils, but are also known to be affected by lithology and redox potential of the source rock depositional environment (Peters et al., 2005). The steranes and triaromatic steroids from different sources exhibit different rates of evolution during the hydrocarbon generation process. For the investigated oils, the values of TA(I)/TA(I + II) and diaC_{27}/regC_{27} steranes vary from

Table 2
Concentrations (ppm, μg/g whole-oil) of steranes for the oil samples.

Sample	S1	S2	S3	S4	S5	S6	S7	S8	S9	S10	S11	S12	S13	S14	S15
1	90	24	74	33	63	47	29	31	32	39	25	54	98	87	55
2	102	32	85	42	84	66	41	38	48	19	31	74	134	125	74
3	19	5	13	5	9	7	4	4	5	5	3	6	12	11	7
4	115	39	98	53	96	75	53	47	52	26	35	90	166	146	95
5	105	32	96	37	74	58	30	22	35	45	18	57	110	101	58
6	105	28	76	35	63	48	36	29	32	19	21	50	93	87	55
7	74	25	58	31	61	48	28	24	35	17	23	58	110	96	56
8	110	29	89	40	82	63	33	36	40	50	26	67	122	110	66
9	75	20	66	30	58	45	30	25	29	36	19	46	88	79	51
10	102	28	80	37	76	58	35	30	35	44	24	55	113	102	54
11	114	35	133	64	120	86	56	58	62	68	38	95	193	167	103
12	85	25	90	41	79	59	41	32	39	37	29	64	124	110	62
13	104	35	102	61	114	88	55	43	56	58	38	92	172	150	97
14	95	38	69	36	60	47	26	22	38	45	27	58	117	100	53
15	96	33	57	30	58	41	28	30	34	34	27	54	97	87	48
16	75	29	46	27	46	33	19	24	27	30	17	45	80	71	36
17	135	41	122	54	109	78	46	37	53	69	32	82	173	147	82
18	87	22	74	26	51	36	24	24	25	36	16	37	75	65	34
19	125	39	103	54	101	74	37	38	53	25	25	75	161	140	78
20	96	23	77	30	56	41	23	25	26	39	17	40	85	72	39
21	87	27	97	43	85	65	43	37	41	43	31	67	132	114	70
22	153	49	120	60	119	93	61	51	70	28	47	107	203	186	114
23	122	42	93	55	97	74	40	21	59	56	34	91	176	150	93
24	103	37	83	40	74	57	39	37	41	42	28	67	122	107	60
25	76	27	63	36	69	53	33	28	35	15	26	63	119	101	59
26	163	62	135	79	153	117	76	64	87	36	58	139	258	223	144
27	199	77	178	115	191	144	86	87	107	108	75	182	317	283	184
28	181	70	149	100	173	140	92	76	103	43	66	162	286	255	162
29	110	40	109	59	117	92	62	43	58	26	38	91	181	157	92
30	184	70	130	71	136	102	65	66	82	41	53	117	226	208	123
31	39	16	28	20	33	25	16	12	19	19	10	30	56	49	30
32	170	61	134	74	144	108	69	65	87	31	59	145	251	234	152
33	113	38	83	54	95	72	42	22	58	59	38	94	177	152	92
34	164	61	124	82	155	115	74	69	91	92	63	144	284	241	137
35	57	22	49	29	55	41	25	26	33	33	23	53	98	88	54
36	144	58	105	77	138	104	59	61	84	84	57	135	239	220	143
37	113	42	90	49	97	71	51	45	59	60	41	102	181	162	104
38	167	59	131	75	147	109	76	69	91	86	59	148	269	238	156
39	198	70	145	95	167	124	77	78	104	103	66	171	313	277	168
40	88	33	71	41	78	57	35	19	50	49	34	82	155	133	75
41	111	39	82	50	93	67	46	50	59	60	39	97	178	158	96
42	140	57	108	68	119	91	57	64	77	78	52	128	229	199	121
43	205	74	144	90	165	120	85	85	103	48	73	180	328	284	185
44	140	54	98	64	112	81	51	58	74	72	49	118	222	190	116
45	119	48	94	57	102	73	47	53	67	63	46	107	200	175	118
46	142	59	104	66	119	89	53	61	74	71	51	123	233	202	132
47	134	47	92	59	105	75	50	34	68	66	46	111	209	179	108
48	203	86	149	88	169	119	74	88	112	107	79	179	335	294	164
EM1	229	113	100	100	155	108	73	99	135	130	98	230	392	339	209
EM2	120	39	112	60	118	90	57	45	62	45	40	99	190	169	106
EM3	80	21	70	27	53	40	24	21	23	27	14	34	69	62	33

Note: The sample information is interpreted in the footnote to Table 1. The EM1, EM2 and EM3 oils are the endmembers and their biomarker concentrations were calculated by ALS-C. S1-S2, C_{21}-C_{22} 5α,14α, 17α(H)-pregnanes (preg); S3, C_{27} 13β(H), 17α(H) 20S + 20R, 13α(H), 17β(H) 20S + 20R-diacholestanes; S4, C_{27} 5α, 14α, 17α(H)-cholestane 20S; S5, C_{27} 5α, 14β, 17β(H)-cholestane 20R; S6, C_{27} 5α,14β,17β(H)-cholestane 20S; S7, C_{27} 5α, 14α, 17α(H)-cholestane 20R; S8, C_{28} 5α, 14α, 17α(H)-ergostane 20S; S9, C_{28} 5α, 14β, 17β(H)-ergostane 20R; S10, C_{28} 5α, 14β, 17β(H)-ergostane 20S; S11, C_{28} 5α, 14α, 17α(H)-ergostane 20R; S12, C_{29} 5α, 14α, 17α(H)-stigmastane 20S; S13, C_{29} 5α, 14β, 17β(H)-stigmastane 20R; S14, C_{29} 5α,14β,17β(H)-stigmastane 20S; S15, C_{29} 5α, 14α, 17α(H)-stigmastane 20R.

0.06 to 0.70 and 0.28 to 0.55, respectively. The samples display two different trends in the cross-plot of these ratios (Fig. 4), indicating that the samples cover the full whole oil window or they are mixtures of oils having different maturities from source rocks of different sedimentary facies.

In most investigated oils from the Tahe oilfield, the entire series of 25-norhopane (25N-Hs), mainly including C_{29}- and C_{28}-norhopanes, C_{30}-C_{34}-norhomohopanes, C_{26}-nortrinorhopanes, occur as well as the 17-nortricyclic terpanes (Fig. 5), indicating that the oils have been exposed to biodegradation in their history (Peters and Moldowan, 1991; Peters et al., 1996). The concentrations of 25N-C_{29}H and 25N-C_{28}H in the oil are within the ranges of 0–169 ppm and 1–535 ppm (Table 3), respectively. The 25N-C_{29}H/C_{30}H ratios range from 0 to 0.45 (Table 1). As *n*-alkanes are the first compound class destroyed by microbes during biodegradation, heavily biodegraded oils generally lack this class of compounds and display a prominent unresolved complex mixture (UCM) hump on GC-FID traces (Peters et al., 2005). Zhang et al. (2014) pointed out that almost all oil samples from the Tarim Basin display biodegradation signatures, including variable UCM and significant amounts of 25-norhopanes. For the investigated oils from the Tahe oilfield, the co-existence of 25-norhopanes, intact *n*-alkanes and UCM indicate that they are mixtures of biodegraded oil with later charge of non-biodegraded oil.

There are generally similar geochemical characteristics between the crude oils from the Tahe oilfield and those in our

Table 3
Concentration (ppm) parameters of terpanes for the oil samples.

Sample	T1	T2	T3	T4	T5	T6	T7	T8	T9	T10	T11	T12	T13	T14	T15	T16	T17	T18	T19	T20	T21	T22	T23
1	52	88	99	37	222	131	115	85	65	82	112	72	92	207	235	198	50	164	90	71	61	57	10
2	60	118	130	51	300	182	159	114	86	114	144	84	143	323	372	383	118	279	150	116	111	112	31
3	16	34	31	11	61	36	27	19	8	15	19	9	11	34	32	24	5	17	8	4	3	13	3
4	66	135	144	59	353	201	178	137	103	131	168	97	166	403	446	440	147	343	170	144	123	139	39
5	68	116	118	44	273	158	132	103	71	102	133	103	91	218	252	203	25	180	102	76	66	45	16
6	56	123	108	38	241	142	128	94	70	101	115	65	84	196	232	202	44	175	73	63	46	76	18
7	38	86	98	38	235	135	124	90	67	88	106	56	118	281	313	297	62	234	117	81	91	108	23
8	76	134	133	48	286	172	140	111	79	111	152	109	89	222	258	202	44	168	95	76	42	34	4
9	50	92	92	33	209	120	104	77	56	79	111	62	59	155	188	148	42	114	61	46	41	21	11
10	66	125	122	47	262	158	136	100	75	111	141	83	72	212	238	183	63	155	84	73	35	41	14
11	83	144	143	49	313	205	189	137	113	172	219	145	101	259	361	352	140	283	130	133	72	33	1
12	60	113	109	36	229	161	135	97	74	121	145	77	65	168	219	221	78	166	63	70	54	24	6
13	64	152	148	58	369	211	190	128	108	148	195	105	152	398	460	441	129	323	148	124	116	1	1
14	47	108	127	48	244	143	125	111	81	95	123	73	78	166	169	122	17	98	63	55	34	346	77
15	48	111	113	39	215	133	114	97	72	95	126	53	79	157	161	128	44	95	66	40	24	325	56
16	36	78	95	34	180	109	93	73	57	66	85	59	55	124	124	87	35	68	44	31	22	276	56
17	96	223	189	67	401	241	207	140	152	161	211	175	126	362	458	364	77	269	136	100	64	57	0
18	65	122	103	39	229	130	104	80	57	77	110	63	28	70	77	55	39	50	22	21	9	40	7
19	109	205	180	68	377	227	189	136	153	135	194	216	133	348	437	321	40	246	185	118	50	70	0
20	75	144	123	46	264	152	117	93	64	91	123	75	31	74	82	55	49	47	28	10	12	54	7
21	68	135	124	51	262	159	138	103	112	120	139	111	171	431	575	484	109	376	200	158	112	37	3
22	66	200	208	84	497	270	246	175	138	174	220	117	229	566	588	604	174	459	228	188	181	177	47
23	60	153	163	68	402	216	197	141	109	135	185	117	202	505	524	477	98	413	215	172	184	128	27
24	52	139	161	59	318	183	169	123	90	119	153	89	76	202	203	192	65	128	71	58	57	290	66
25	39	99	115	42	254	144	128	93	81	97	122	74	177	328	349	346	101	259	134	107	86	138	33
26	79	218	253	95	553	322	294	212	174	230	260	167	311	734	776	755	187	549	291	247	220	313	84
27	90	267	328	129	740	420	379	274	226	276	362	247	363	900	937	802	193	652	356	293	278	492	139
28	70	231	287	113	675	370	339	247	189	249	318	160	352	835	797	733	196	583	277	248	259	529	147
29	74	164	154	60	364	213	183	132	131	147	187	137	183	477	602	552	105	404	205	167	128	41	14
30	70	203	246	105	630	341	282	206	174	178	243	134	299	702	724	678	107	527	268	227	224	138	26
31	22	42	51	21	122	72	61	45	37	44	60	31	61	145	159	140	22	113	69	66	49	47	13
32	64	217	247	103	615	329	291	208	163	204	261	147	316	794	802	774	165	629	317	253	292	264	54
33	44	123	151	66	379	202	191	137	100	116	167	109	216	527	533	498	80	415	233	166	203	164	53
34	69	169	231	98	589	324	292	216	162	191	268	154	334	796	841	753	114	616	323	261	266	264	87
35	25	64	84	36	214	118	111	78	61	70	92	59	121	289	301	272	61	226	118	92	102	100	31
36	52	155	208	87	527	291	257	193	144	176	233	154	316	738	759	694	158	563	300	240	254	272	80
37	40	135	163	67	416	218	201	146	105	142	176	90	241	541	539	544	144	428	222	188	202	232	65
38	64	205	232	104	614	326	309	212	153	195	249	134	365	796	770	805	228	622	313	260	307	347	82
39	72	189	271	120	667	367	349	247	188	204	288	198	419	923	939	840	204	698	389	298	329	427	126
40	32	100	128	56	328	178	162	117	88	105	137	85	198	441	442	399	87	326	176	144	157	217	60
41	34	123	152	69	392	211	194	145	107	119	163	107	239	523	511	487	112	406	218	164	198	253	86
42	47	157	204	86	503	271	252	181	134	150	211	128	307	664	654	601	142	496	257	197	244	349	105
43	67	222	280	116	715	376	349	249	187	232	296	153	417	948	904	948	194	721	372	288	360	498	135
44	41	146	190	83	487	255	248	170	126	144	201	130	289	635	615	581	137	484	261	199	243	346	103
45	41	136	176	74	451	237	221	156	121	128	185	118	264	582	559	534	124	444	248	193	222	321	99
46	49	158	204	87	524	273	259	183	138	146	215	140	301	671	632	610	145	504	279	224	247	375	117
47	42	131	179	81	458	244	234	165	120	134	184	121	271	599	579	539	131	447	247	191	229	340	103
48	64	225	287	121	722	396	362	269	203	217	309	197	428	959	886	983	99	712	364	304	367	535	169
EM1	0	171	357	159	892	440	445	333	194	209	310	137	603	1198	865	912	192	750	427	330	515	1521	424
EM2	71	160	163	67	411	234	206	144	128	153	196	133	223	557	649	603	133	473	241	195	177	0	0
EM3	65	114	96	31	178	117	93	73	59	85	109	73	1	28	70	29	27	19	11	10	0	39	0

Note: The sample information is interpreted in the footnote to Table 1. T1-T8, C_{19}-C_{26} tricyclic terpanes (TT); T9, C_{24} tetracyclic terpane (C_{24}Te); T10-T11, C_{28}, C_{29} tricyclic terpanes; T12, 18α(H), 21β-22,29,30-trinorneohopane (Ts); T13, 17α(H), 21β-22,29,30-trinorhopane (Tm); T14, C_{29} hopane (C_{29}H); T15, C_{30} hopane (C_{30}H); T16, C_{31} homohopanes 22S + 22R (C_{31}H); T17, gammacerane (G); T18, C_{32} bishomohopanes 22S + 22R (C_{32}H); T19, C_{33} trishomohopanes 22S + 22R (C_{33}H); T20, C_{34} tetrakishomohopanes 22S + 22R (C_{34}H); T21, C_{35} pentakishomohopanes 22S + 22R (C_{35}H); T22, 25-nor C_{28} hopane (25N-C_{28}H); T23, 25-nor C_{29} hopane (25N-C_{29}H).

our previous study (Zhan et al., 2016a) from the whole Tabei Uplift, although the samples analyzed were different. Like the samples from the Tabei Uplift (Zhan et al., 2016a), the Tahe oilfield oils are mixtures of different hydrocarbons from the ϵ-O_1 and O_{2-3} source rocks at different maturities.

4.2. De-convoluting mixed oils

4.2.1. The number of endmembers

Like the Tabei Uplift marine oils (Zhan et al., 2016a), the number of endmembers was identified as three for the samples from the Tahe oilfield based on ALS and geological input. The cumulative variance achieved 99.7% using three sources, satisfying the requirements of multivariate statistical analysis (generally not less than 90%). When the assumed number of endmembers is increased to more than three, the resulting changes in the cumulative variances are minor. Therefore, three endmembers are sufficient, mathematically, to represent the chemical variations measured within our sample set. It is supported by previous studies which verified that oils from Palaeozoic reservoirs in the Tarim Basin originated from the ϵ-O_1 and O_{2-3} source rocks having different maturities (Li et al., 2010b, 2015a,b; Yu et al., 2011, 2012; Tian et al., 2012a,b; Zhu et al., 2013).

4.2.2. Geological significance of endmembers

The compound compositions of the three endmember oils (EM1, EM2, EM3) were predicted by ALS-C using a dataset of 38 concentration parameters and are shown in Tables 2 and 3. Some biomarker ratios of endmember oils were obtained using related compound concentrations computed by ALS-C.

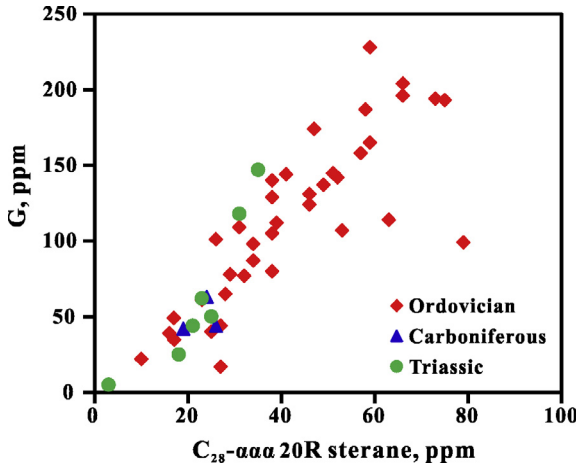

Fig. 3. Plot of the concentrations of gammacerane (G) and C_{28}-ααα 20R sterane of the oils.

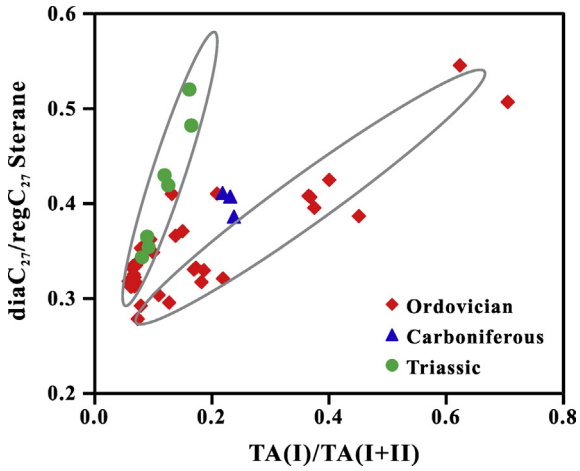

Fig. 4. Correlations of ratios of TA(I)/TA(I + II) vs. $diaC_{27}/regC_{27}$ steranes of the oils.

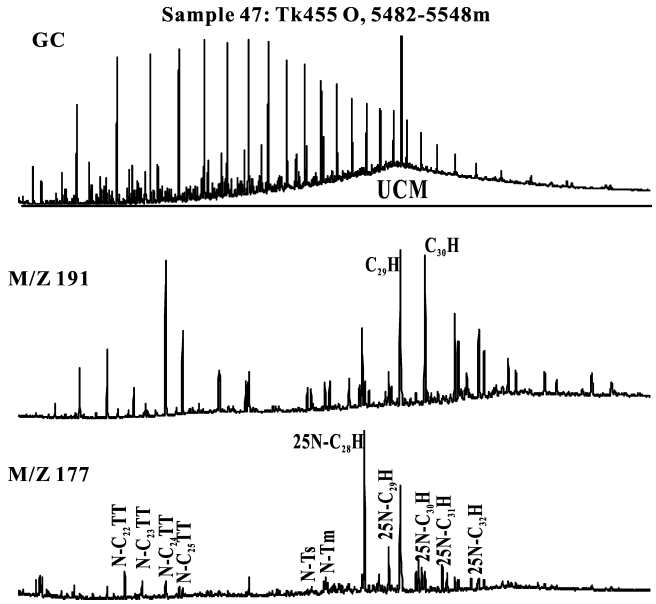

Fig. 5. Whole oil gas chromatogram (GC), m/z 191 and 177 mass chromatogram of the sample 47 in the Tahe oilfield show the co-existence of intact *n*-alkane series, UCM and 25-norhopanes.

The EM1 oil has the highest concentrations of C_{27}-C_{29} steranes, C_{29} hopane ($C_{29}H$), C_{35} homohopane ($C_{35}H$) and gammacerane (G) and low relative abundances of tricyclic terpanes. Ratios of $C_{29}H/C_{30}H$, $C_{35}H/C_{34}H$ and $G/C_{30}H$ are 1.38, 1.56 and 0.22, respectively. The normalized relative contents of C_{27}, C_{28}, C_{29}-ααα 20R steranes are 0.19, 0.26, and 0.55, respectively. Ratios of C_{29} sterane 20S/(S + R) and ββ/(ββ + αα) are 0.52 and 0.62, respectively, approaching to their endpoints. Compared to the regular steranes, EM1 has relative low abundances of pregnanes and diasteranes. All of these biomarker parameters indicate that the EM1 oil was generated in the early to peak oil window from source rock organic matter composed mainly of algae, deposited in a restricted, clay poor, hypersaline marine environment. These geochemical characteristics correspond to those of the $Є$-O_1 source rocks in the Tarim Basin. Therefore, it can be concluded from ALS-C that the EM1 contribution to the Tahe oilfield mixed oils originated from $Є$-O_1 source rocks in the early to peak oil window. EM1 has the highest concentration of 25-norhopane ($25N\text{-}C_{29}H$) and $25N\text{-}C_{29}H/C_{30}H$ reaches to 0.50, suggesting that it was also very heavily biodegraded.

The C_{29} 20S/(S + R) and ββ/(ββ + αα) sterane ratios are 0.48 and 0.64 for EM2, which are similar to the results for EM3(0.52 and 0.66). However, EM2 has slightly lower ratios of $diaC_{27}/regC_{27}$ and Ts/(Ts + Tm) than EM3. The contributions of EM2 to the sample 21 (TK1138 oil) and EM3 to the sample 20 (S112 oil) are 99% and 97% (Table 4), respectively. Samples of 21 and 20 can represent the EM2 and EM3 oils, respectively. The values of TA(I)/TA(I + II) are 0.21 for the sample 21 and 0.70 for the sample 20 (Table 1). These features reveal that the EM2 oil has lower maturity than the EM3 oil. This is also verified by the concentrations of biomarkers not affected by thermal effects, even though the oils are affected by other processes (such as biodegradation). For example, the tricyclic terpanes and steranes have higher thermal stability than pentacyclic terpanes (Peters et al., 2005). The EM3 oil has few and incomplete pentacyclic terpanes, but relatively higher concentrations of tricyclic terpanes and steranes, which is the opposite of the EM2 oil (Tables 2 and 3). In addition, biodegradation also enriched biomarkers in EM2 and led to differences in some parameters for the two EM oils because the steranes and tricyclic terpanes are more resistant to biodegradation than the hopanes.

Despite the different maturities for EM2 and EM3, source-related biomarkers (*i.e.*, those sensitive to depositional environment of the source rock) suggest that these two endmembers are from a similar source. Both show a "V" shape distribution of C_{27}, C_{28}, C_{29}-ααα 20R steranes and almost the same normalized relative abundances, 0.30, 0.18, 0.52 and 0.34, 0.19, 0.47 for the EM2 and EM3 oils respectively, indicating that their source rocks contain similar organic matter. They have no elevated $C_{29}H$ and $C_{35}H$ and ratios of $C_{29}H/C_{30}H$ and $C_{35}H/C_{34}H$ are less than 1. The relative abundances of pregnanes and diasteranes in the EM2 and EM3 oils are higher than those in the EM1 oil. These characteristics suggest that their source rocks were deposited in an open and sub-oxic marine environment. The inferred environmental conditions under which the source rocks for EM2 and EM3 were deposited are similar to that of the O_{2-3} source rocks in the Tarim Basin. Therefore, it seems reasonable to conclude that the EM2 and EM3 oils originated from O_{2-3} source rocks in the Tabei region and the former was generated in the early to peak oil window, while the latter was from the late oil generation stage.

4.2.3. Distributions of endmembers

The relative contributions of the three endmembers to the Tahe oilfield oils were calculated by ALS-C and are listed in Table 4. EM1 is a minor contributor to the mixed oil samples with an average of 13%. EM2 is the major contributor with an average of 52% and its

Table 4
The fractional contributions of endmembers to crude oil samples calculated by ALS-C.

Sample.	Well	Reservoir	Depth, m	Density g/cm^3	EM1, %	EM2, %	EM3, %
1	AT2-5	T	4029–4033	0.87	4	36	60
2	AT1-13H	T	/	0.85	8	55	37
3	AT9-1H	T	4608–4718	0.79	3	10	87
4	YT2-13	T	/	0.85	9	58	33
5	TK203	T	4593–4597	0.83	2	30	68
6	TK7208	T	4412–4415	0.84	4	28	68
7	TK103	T	4514–4576	0.90	12	63	25
8	TK305	C	5231–5239	0.84	1	27	72
9	S70	C	5153–5168	0.83	1	27	72
10	TK310	C	5016–5019	0.82	1	27	72
11	S89	O	5519–5550	0.86	0	37	63
12	S68	O	/	0.82	0	29	71
13	S7204	O	5783–6124	0.83	0	60	40
14	AT35	O	5737–5855	0.85	20	0	80
15	TK515	O	5471–5520	0.86	20	0	80
16	TK515	O	/	0.86	21	0	79
17	TP204	O	6348–6410	0.83	0	36	64
18	TK1118X	O	6231–6249	0.83	1	4	95
19	TP308X	O	6584–6679	0.84	1	35	64
20	S112	O	6172–6189	0.83	1	2	97
21	TK1138	O	5936–6019	0.84	1	99	0
22	TK720	O	6120–6231	0.91	9	61	30
23	TK835	O	5765–5840	0.93	9	72	19
24	TP129	O	6614–6682	0.91	15	0	85
25	TH10419	O	6068–6148	0.92	15	69	16
26	TP103	O	6130–6218	0.91	15	66	19
27	TP106	O	6299–6365	0.93	17	47	36
28	TH10303	O	6084–6179	0.95	22	44	34
29	T701	O	/	0.84	1	84	15
30	TK707	O	5708–5767	0.98	7	66	27
31	S46	O	5373–5455	0.96	10	60	30
32	TK882	O	5727–5765	0.87	14	79	7
33	TK842	O	5528–5620	0.93	15	85	0
34	TK349	O	5373–5428	0.87	15	83	2
35	TK231	O	5550–5585	0.92	16	81	3
36	TK315	O	5431–5498	0.94	18	82	0
37	TK729	O	/	0.97	20	80	0
38	TK822	O	5631–5632	0.95	20	78	2
39	TK537	O	5387–5452	0.92	23	77	0
40	S48	O	5363–5370	0.96	24	73	3
41	TK644	O	5565–5607	0.96	24	74	2
42	TK210	O	5448–5560	0.98	25	66	9
43	TK626	O	/	0.97	26	74	0
44	TK634	O	5567–5599	0.97	26	67	7
45	TK469	O	5562–5620	0.97	27	66	7
46	TK469	O	5548–5560	0.95	26	63	11
47	TK455	O	5482–5548	0.97	28	65	7
48	S65	O	5451–5585	0.97	28	69	3

proportion ranges from 0% to 99%. EM3 is the secondary contributor with a range of 0–97% and an average of 35%.

The relative contributions of the endmembers are marked in Fig. 6. Besides the oils from the eastern region of the Tahe oilfield, the proportions of the EM1 and EM2 oils gradually increase from south to north and east to west, while that of the EM3 oil is gradually reduced. These trends hint that the three endmembers have a similar filling orientation and pathway. Mixing of oils from different filling stages can occur when late oil migrates into the same reservoir (*i.e.*, Ordovician reservoirs) along the migration pathway of an earlier oil. Late charge oil occupies the most favorable and the nearest reservoir spaces away from the filling points by mixing and/or displacement of the early oil. Consequently, the proportion of early oil increases along the charge pathway, while that of late oil decreases. There are a few samples (*e.g.*, AT35 and TK103 wells) from the northeast region that deviate from these trends (Fig. 6), indicating different mechanism of charging and mixing (discussed in Section 4.3).

The EM1 oil suffered very heavy biodegradation and has high density. The EM2 oil generated in the early oil generation stage has relatively higher density than the EM3 oil that was expelled in the late oil window. Therefore, density is expected to decrease with increasing proportions of EM3 and to increase with increasing EM1 (Fig. 7). This can be used to explain the observation that crude oils from the Tahe oilfield, except for a few samples from the eastern area, have greatly varied densities, ranging from 0.79 to 0.98 g/cm^3, which also show a gradually increasing trend from south to north and east to west (Fig. 8).

4.3. Multiple charging and mixing

4.3.1. Orientation and pathway of oil filling

Owing to the strong interaction between polar nitrogen compounds and clay minerals and/or solid organic matter that results in geo-chromatographic fractionation, the concentration of pyrrolic nitrogen compounds (carbazoles) in crude oil is expected to decrease along the oil migration pathway and carbazoles are useful tracers for reconstruction of the reservoir filling process (Li et al., 1995; Stoddart et al., 1995; Larter et al., 1996; Wang et al., 2005). Dibenzothiophenes (DBTs) and dibenzofurans (DBFs) have the same molecular structure and characteristics as carbazoles, so they can also produce a migration fractionation effect similar

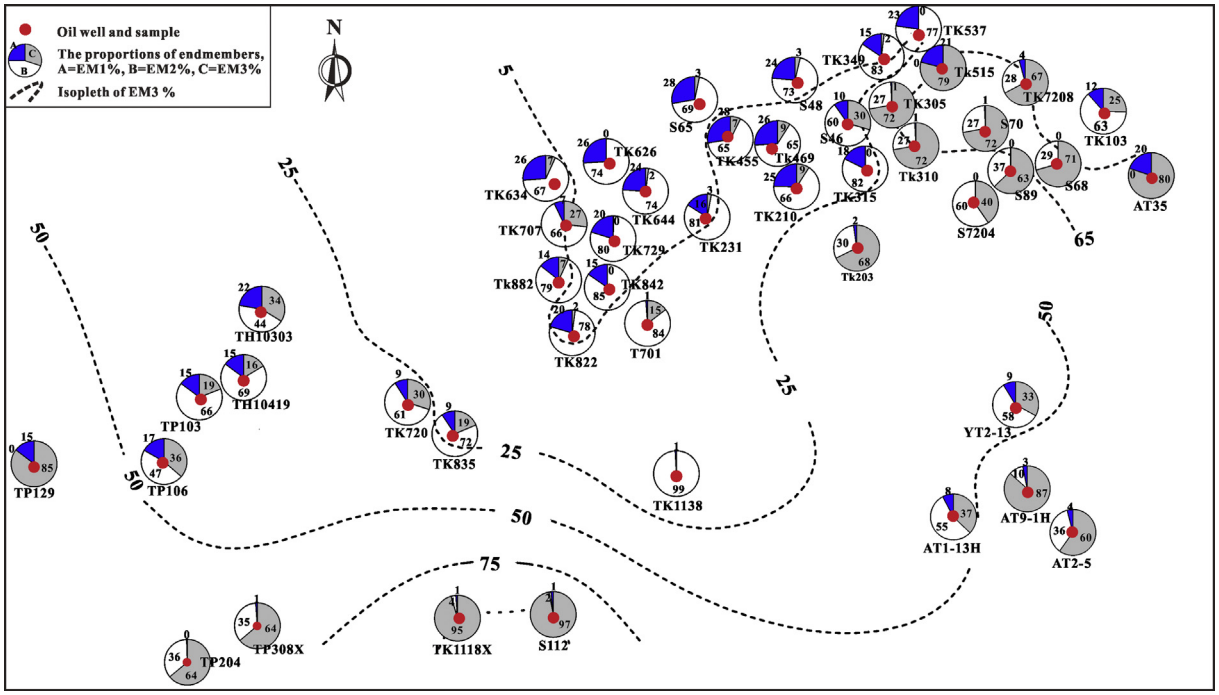

Fig. 6. Distribution of the relative contributions of the three endmember (EM) oils and isopleth of the EM3.

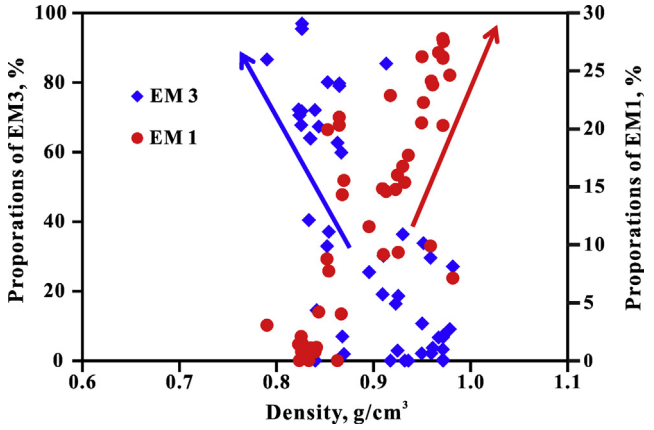

Fig. 7. Cross-plots of relative density versus the relative proportions of EM3 and EM1.

to that of carbazoles during oil migration based on the hydrogen bond mechanism and the polarity caused by dipoles (Wang et al., 2005; Li et al., 2011). The relative and total abundances of DBTs and DBF's, like carbazoles, are potentially useful indicators of oil migration and reservoir filling pathways (Wang et al., 2005; Li et al., 2008, 2011; Zhang et al., 2012), although complications can arise from factors such as source facies variability and thermal maturation.

In this study, the proposed filling pathway for the Tahe oilfield is summarized on a map by plotting the total concentrations of DBTs (the sum of dibenzothiophene, methyl dibenzothiophenes, and dimethyl dibenzothiophenes) and DBFs (the sum of dibenzofuran, methyl dibenzofurans and dimethyl dibenzofurans) (Fig. 9). The direction of decreasing total concentration isopleths indicates the preferential oil migration direction and filling pathway. Fig. 9 shows that the general oil filling orientations are from south to north and from east to west. Huang (2003) and Gu et al. (2003) reached a similar conclusion based on observations of regional trends in physical properties, light hydrocarbons, biomarkers and nitrogenous compounds in crude oils. Geologically, the Tahe oilfield is bounded by the Canhu Depression to the east and the Manjiaer Depression to the south (Fig. 1), where Lower Palaeozoic source rocks are well developed (Zhang et al., 2004). These depression/sags were considered as source kitchens for the Tahe oilfield (Huang, 2003; Gu et al., 2003). However, Wang et al. (2008) argued that the Shuntuoguole Uplift to the south of the Tahe oilfield is the most probable source kitchen, based on molecular parameters and total concentrations of pyrrolic nitrogen compounds. In the south-north transect, a main oil stringer migrated from filling point TK1118X-S112-TK1138. The contributions of the three endmembers (EM1, EM2, EM3) are 1%, 3%, 96% to sample 18, 1%, 2%, 97% to sample 20, and 1%, 99%, 0 to sample 21, respectively. One scenario that would explain these observations is that the first charged oil (EM1) was mixed or replaced by the second charged oil (EM2), and then mixed or displaced by the third charged oil (EM3), leaving tiny amounts of early charged oil (EM1 and EM2). The third charged oil may have followed a detour around well TK1138, resulting in no EM3 oil in the reservoir.

Although the general tread of DBTs and DBFs concentrations gradually decreases from east to west, a few samples in the north-east region are outliers, indicating a different charging and mixing model, which is similar to the distribution of the relative contributions of the three endmembers. Vertically, three reservoirs occur in the eastern region of the Tahe oilfield, including Ordovician, Carboniferous and Triassic. During the course of tectonic evolution of the basin, there is the potential for destruction of certain reservoirs, allowing subsequent re-migration and accumulation in a secondary reservoir. The generation and expulsion of the EM1 and EM2 oils was earlier than the formation of Triassic clastic rock reservoirs and/or traps. Yu et al. (2011, 2012) showed that the absorbed and inclusion oils from clastic reservoirs in the Tahe oilfield are similar, indicating they are charged into the reservoir at the same time, and have higher relative concentrations of gammacerane and C_{28}-ααα 20R sterane and higher $\delta^{13}C$ values than the free oils. They suggested that the absorbed and inclusion

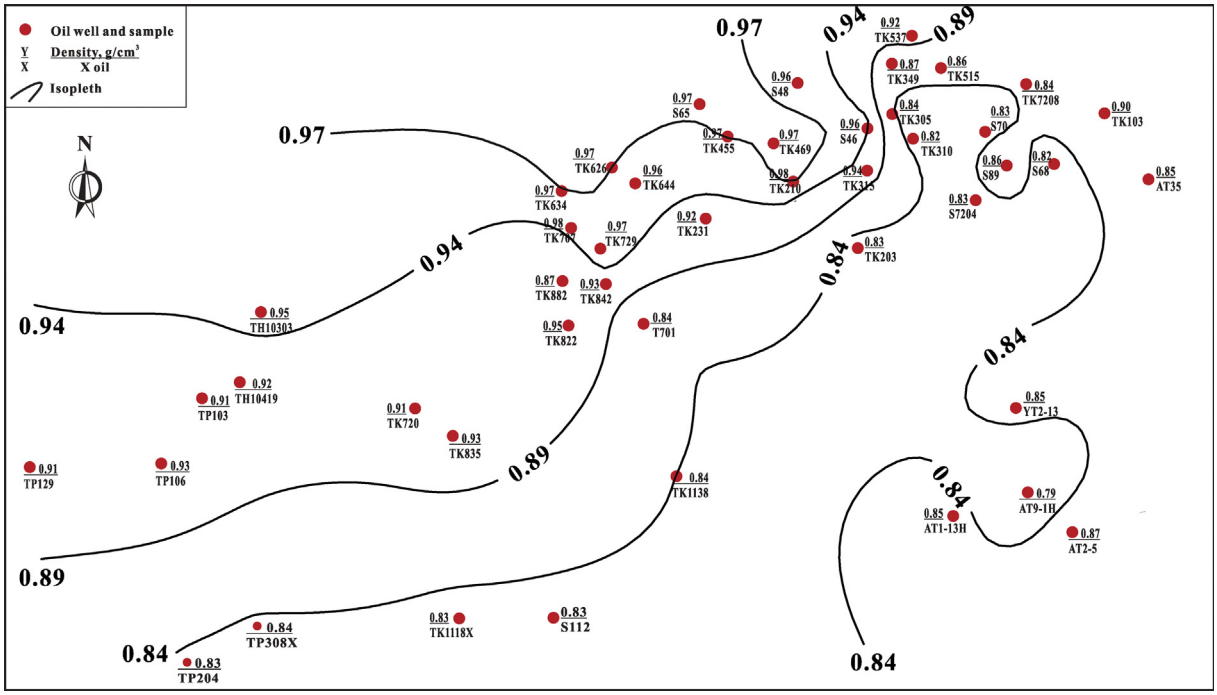

Fig. 8. Isopleth map showing variations in oil density.

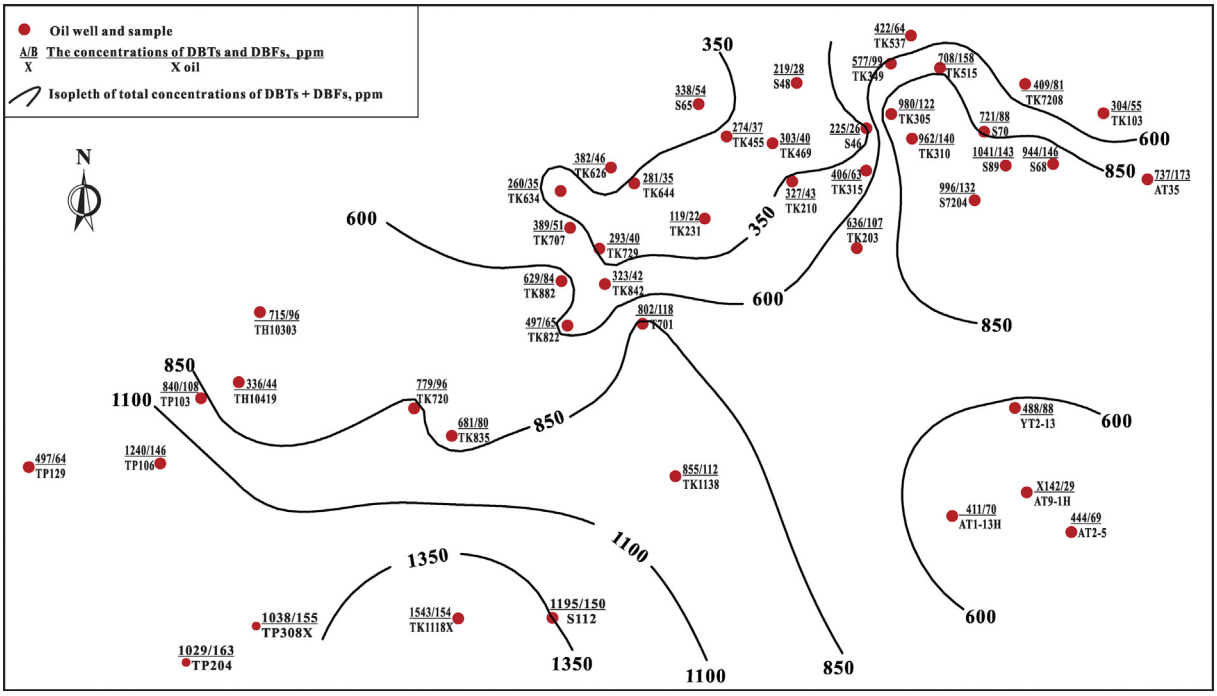

Fig. 9. Concentration distribution of dibenzothiophenes (DBTs) and dibenzofurans (DBFs) and isopleths of their total concentration (DBTs + DBFs).

oils represent a mixture from two source rocks (one of them might be ϵ-O_1 source rocks), but that the free oils originated from one source rock at a higher maturity level. The sandstone reservoirs in the Tahe oilfield experienced two oil charges (Wang et al., 2004, 2008) and the first charge contained components derived from the ϵ-O_1 source rocks (Yu et al., 2011, 2012). Therefore, it can be postulated from these observations that theses first charged mixtures of the EM1 and EM2 oils and they accumulated in lower reservoirs (Ordovician and/or Carboniferous) initially. These reservoirs were subsequently destroyed, causing upward remigration and re-accumulation of the EM1 and EM2 oils in the upper reservoirs. This mixed phase was finally mixed with EM3 oil in Triassic reservoirs.

4.3.2. Model of multiple charging and mixing

The burial and geothermal histories of different tectonic units of the Tarim Basin were reported previously (Cai et al., 2001; Zhang et al., 2004; Li et al., 2010a). The ϵ-O_1 source rocks show more rapid sedimentation and burial than the O_{2-3} source rocks, leading to more rapid organic matter maturation and petroleum

generation (Cai et al., 2009). The ϵ-O_1 source rocks reached peak oil generation by the Caledonian Period, the wet gas stage by the late Hercynian Period, and were already overmature during the Himalayan Period, generating only dry gas (Zhang et al., 2004). As a result of uplift during the later Caledonian-early Hercynian and subsidence during the Permian, the O_{2-3} source rocks reached the oil generation stage in the late Hercynian Period, and are still within the mature to overmature stage due to a combination of uplift during the period from the late Permian to the Eocene and heat flow decrease since the Triassic (Zhang et al., 2004; Li et al., 2010a). Considering the histories of sedimentary tectonic evolution in the study areas, hydrocarbon generation and expulsion from the two marine source rocks and the relative contributions and component characteristics of the three endmember oils from ALS-C, a model of three oil charges and two mixing events can be postulated for the Tahe oilfield oils.

The first charge took place during the Caledonian orogeny. The middle-lower Ordovician karst reservoirs developed before early Silurian and were capped by argillaceous rocks, forming the early Palaeozoic reservoir-seal assemblage. At that time, the ϵ-O_1 source rocks reached peak oil generation, while the O_{2-3} source rocks were still immature. Abundant petroleum from the ϵ-O_1 source rocks charged the Ordovician reservoirs from south to north and/or east to west. As a result of sedimentary discontinuity and denudation by crustal uplift during the late Caledonian to the early Hercynian, the oils were very heavily biodegraded, forming 25-norhopanes and residual heavy oil in the reservoir.

The second charge and first mixing event occurred during the late Hercynian orogeny. The lower Palaeozoic carbonate reservoirs further developed by karstification in the late Caledonian to the early Hercynian, and were then covered by the Carboniferous regional seal in the middle Hercynian. By the end of the Permian Period, large amounts of hydrocarbons generated from the O_{2-3} source rocks in the early oil generation stage charged the Palaeozoic reservoirs and mixed with the residual oils from the first charge. Subsequent compressional uplift in the late Hercynian exposed the mixtures to biodegradation.

The third charge and second mixing event took place during the late Yanshan to the Himalayan orogeny. Continental sedimentation occurred in the Tabei area upon entering the Mesozoic Era and the structural topography was gradually reversed, forming a series of faults and traps. In some areas, the Paleozoic reservoirs were destroyed and petroleum migrated along faults into the upper reservoirs (*e.g.,* Triassic clastic rock reservoir) and re-accumulated. During the Himalayan (probably the Miocene to Pliocene) (Wang et al., 2008), large quantities of petroleum from the O_{2-3} source rocks in the late oil generation stage, as well as pre-mixed oils, migrated along unconformities and faults into favorable reservoirs. This oil mixed with and displaced previously mixed oils, and continued to migrate from south to north or east to west. The final mixtures were likely affected by local secondary processes, such as evaporative fractionation or gas washing (Zhu et al., 2013).

The Tahe oilfield is in a local structure (the Akekule High) of the Tabei Uplift (Fig. 1). The formation models of mixed oil for these two regions are generally similar (Zhan et al., 2016a). However, regional differences can be observed for the relative contribution of endmembers. For example, the EM2 oil that originated from O_{2-3} source rocks in the early oil generation stage is the major contributor to the Tahe oilfield mixed oils, but only a secondary contributor to the Tabei Uplift mixtures, while the EM3 oil is the opposite. Reasons for these differences may include variations in the structure type and location, filling orientation and pathway, sedimentary microfacies of source rock, and the degree and type of secondary alteration.

5. Conclusions

The Tahe oilfield comprises multi-layered oil pays in Ordovician (karst), Carboniferous and Triassic (clastic rock) reservoirs characterized by co-existing types of crude oils, including heavy, normal, and light oil, and condensate. Their stable carbon isotope compositions suggest marine organic matter sourced crude oils. These oils were subjected to different types and degrees of secondary alteration deduced from the complete but varied distribution patterns of paraffinic hydrocarbons with widely variable bulk characteristics. However, based on distributions of biomarkers and aromatic hydrocarbons in the crude oils, we conclude that they are mixtures of hydrocarbons having different maturities that were derived from source rocks deposited in different marine sedimentary facies. The inferred source rock intervals are the ϵ-O_1 and O_{2-3} source rocks in the Tabei area in the Tarim Basin.

Chemometric analysis by alternating least squares of 38 concentration parameters (ALS-C) for the 48 oil samples identifies three endmember (EM) oils. EM1 is a minor contributor with an average of 13%, which originated from the ϵ-O_1 source rocks in the mature to peak hydrocarbon generation stage. EM1 experienced two phases of mixing and biodegradation. EM2 is a major contributor with an average of 52%. The EM2 oil originated from O_{2-3} source rocks in the early oil generation stage and underwent two phases of mixing and one stage biodegradation. EM3 is a secondary contributor with average of 35%. The EM3 oil was also generated from O_{2-3} source rocks, but in the late oil widow. EM3 mixed with earlier emplaced mixtures in the reservoirs. The general orientation and pathway of oil filling was from south to north and east to west. The final mixtures formed by three stages of charge and two mixing and biodegradation events are currently being produced from the Tahe oilfield. We infer inputs from multiple marine source rocks based on deconvolution of biomarker distributions in these mixed phases and attempt to quantify local variations in the relative proportion of these source inputs. Secondary alteration processes (*e.g.* biodegradation, gas washing and evaporative fractionation) that affected these components individually (before mixing) or as mixed phases are inferred from the distribution patters of paraffinic hydrocarbons. These post accumulation alteration mechanisms vary locally in response to geologic factors.

Acknowledgements

We are grateful to Drs. Kenneth E. Peters, Erdem Idiz and two other anonymous reviewers for their constructive suggestions and comments that significantly improved the quality of this manuscript. We thank Drs. Shuang Yu, Yankuan Tian and Long He for providing some samples. The CNPC-CAS strategic cooperation project (Grant No. RIPED-2015-JS-255), NSFC (Grant Nos. 41273059 and 41173054), and SKLOG Project (Grant Nos. skloga201601 and sklogc201604) are acknowledged for financial support. This is contribution No. IS-2373 from GIGCAS.

Associate Editor—**Kenneth Peters**

References

Cai, C.F., Hu, W.S., Worden, R.H., 2001. Thermochemical sulphate reduction in Cambro-Ordovician carbonates in Central Tarim. Marine and Petroleum Geology 18, 729–741.

Cai, C., Li, K., Anlai, M., Zhang, C., Xu, Z., Worden, R.H., Wu, G., Zhang, B., Chen, L., 2009. Distinguishing Cambrian from Upper Ordovician source rocks: evidence from sulfur isotopes and biomarkers in the Tarim Basin. Organic Geochemistry 40, 755–768.

Connan, J., Cassau, A.M., 1980. Properties of gases and petroleum liquids derived from terrestrial kerogen at various maturation levels. Geochimica et Cosmochimica Acta 44, 1–23.

Gu, Y., Huang, J., Shao, Z., 2003. Petroleum geochemistry and hydrocarbon migration in the Tahe oilfield of the Tarim Basin. Petroleum Geology & Experiment 25, 746–750 (in Chinese with English abstract).
Huang, H., Zhang, S., Su, J., 2016. Palaeozoic oil–source correlation in the Tarim Basin, NW China: a review. Organic Geochemistry 94, 32–46.
Huang, J., 2003. An approach to the application of biomarkers to the migration of crude oil in Tahe oil district of Tarim Basin. Petroleum Geology & Experiment 25, 573–576 (in Chinese with English abstract).
Jia, W., Wang, Q., Peng, P.a., Xiao, Z., Li, B., 2013. Isotopic compositions and biomarkers in crude oils from the Tarim Basin: oil maturity and oil mixing. Organic Geochemistry 57, 95–106.
Larter, S.R., Bowler, F., Li, M., et al., 1996. Benzocarbazoles as molecular indicators of secondary oil migration distance. Nature 383, 593–599.
Li, M., Larter, S.R., Stoddart, D., Bjorøy, M., 1995. Fractionation of pyrrolic nitrogen-compounds in petroleum during migration: direction of migration-related geochemical parameters. In: Cubitt, J.M., England, W.A. (Eds.), The Geochemistry of Reservoirs. Geological Society Special Publication 86. Geological Society, London, pp. 103–123.
Li, M., Wang, T., Chen, J., He, F., Yun, L., Akbar, S., Zhang, W., 2010a. Paleo-heat flow evolution of the Tabei Uplift in Tarim Basin, northwest China. Journal of Asian Earth Sciences 37, 52–66.
Li, M., Wang, T.-G., Liu, J., Zhang, M., Lu, H., Ma, Q., Gao, L., 2008. Total alkyl dibenzothiophenes content tracing the filling pathway of condensate reservoir in the Fushan Depression, South China Sea. Science in China (D) 51, 138–145 (in Chinese).
Li, M., Wang, T.-G., Yang, F., Shi, Y., 2011. Molecular markers for tracing light oil and condensate reservoirs filling pathway: alkyl dibenzofurans. Journal of Oil and gas Technology 33 (3), 6–11 (in Chinese with English abstract).
Li, S., Pang, X., Jin, Z., Yang, H., Xiao, Z., Gu, Q., Zhang, B., 2010b. Petroleum source in the Tazhong Uplift, Tarim Basin: new insights from geochemical and fluid inclusion data. Organic Geochemistry 41, 531–553.
Li, S., Pang, X., Zhang, B., Sun, H., Sun, A., 2015a. Marine oil source of the Yingmaili oilfield in the Tarim Basin. Marine and Petroleum Geology 68 (Part A), 18–39.
Li, S., Amrani, A., Pang, X., Yang, H., Said-Ahmad, W., Zhang, B., Pang, Q., 2015b. Origin and quantitative source assessment of deep oils in the Tazhong Uplift, Tarim Basin. Organic Geochemistry 78, 1–22.
Anlai, Ma, Shuichang, Zhang, Dajiang, Zhang, Zhijun, Jin, 2004. Oil and source correlation in Lunnan and Tahe heavy oil fields. Oil and Gas Geology 25, 31–38 (in Chinese with English abstract).
Peters, K.E., Moldowan, J.M., 1991. Effects of source, thermal maturity, and biodegradation on the distribution and isomerization of homohopanes in petroleum. Organic Geochemistry 17, 47–61.
Peters, K.E., Moldowan, J.M., McCaffrey, M.A., Fago, F.J., 1996. Selective biodegradation of extended hopanes to 25-norhopanes in petroleum reservoirs. Insights from molecular mechanics. Organic Geochemistry 24, 765–783.
Peters, K.E., Walters, C.C., Moldowan, J.M., 2005. The Biomarker Guide. Cambridge University Press, Cambridge.
Peters, K.E., Scott Ramos, L., Zumberge, J.E., Valin, Z.C., Scotese, C.R., Gautier, D.L., 2007. Circum-Arctic petroleum systems identified using decision-tree chemometrics. American Association of Petroleum Geologists Bulletin 91, 877–913.
Peters, K.E., Scott Ramos, L., Zumberge, J.E., Valin, Z.C., Bird, K.J., 2008. De-convoluting mixed crude oil in Prudhoe Bay Field, North Slope, Alaska. Organic Geochemistry 39, 623–645.
Peters, K.E., Coutrot, D., Nouvelle, X., Ramos, L.S., Rohrback, B.G., Magoon, L.B., Zumberge, J.E., 2013. Chemometric differentiation of crude oil families in the San Joaquin Basin, California. American Association of Petroleum Geologists Bulletin 97, 103–143.
Peters, K.E., Wright, T.L., Ramos, L.S., Zumberge, J.E., Magoon, L.B., 2016. Chemometric recognition of genetically distinct oil families in the Los Angeles basin, California. American Association of Petroleum Geologists Bulletin 100, 115–135.
Stoddart, D.P., Hall, P.B., Larter, S.R., Brasher, J., Li, M., Bjoroy, M., 1995. The reservoir geochemistry of the Eldfisk Field, North Sea. In: Cubitt, J.M., England, W.A. (Eds.), The Geochemistry of Reservoirs, 86. Geological Society Special Publication, Geological Society, London, pp. 257–279.
Sun, Y., Xu, S., Lu, H., Cai, P., 2003. Source facies of the Paleozoic petroleum systems in the Tabei uplift, Tarim Basin, NW China. Organic Geochemistry 34, 629–634.
Sofer, Z., 1984. Stable carbon isotope compositions of crude oils; application to source depositional environments and petroleum alteration. American Association of Petroleum Geologists Bulletin 68, 31–49.
Tao, G., Qin, J., Tun, G., Zhang, M., Fu, X., Lou, Z., 2010. Comparative study of geochemistry and multivariate data analysis on mixed oils accumulated in Ordovician reservoir in Tahe Oilfield, Tarim Basin, NW China. Geological Journal of China Universities 16 (4), 527–538 (in Chinese with English abstract).
Tian, Y., Zhao, J., Yang, C., Liao, Z., Zhang, L., Zhang, H., 2012a. Multiple-sourced features of marine oils in the Tarim Basin, NW China – geochemical evidence from occluded hydrocarbons inside asphaltenes. Journal of Asian Earth Sciences 54–55, 174–181.
Tian, Y., Yang, C., Liao, Z., Zhang, H., 2012b. Geochemical quantification of mixed marine oils from Tazhong area of Tarim Basin, NW China. Journal of Petroleum Science and Engineering 90–91, 96–106.
Wang, T.-G., Wang, C., He, F., Wang, J., Zhu, D., Wang, C., Xie, M., 2004. Determination of double filling ratio of mixed crude oils in the Ordovician oil reservoir, Tahe oilfield. Petroleum Geology & Experiment 26 (1), 74–79 (in Chinese with English abstract).
Wang, T.-G., He, F., Li, M., Hou, Y., Guo, S., 2005. Alkyldibenzothiophenes: molecular tracers for filling pathway in oil reservoirs. Chinese Science Bulletin 49, 2399–2404 (in Chinese).
Wang, T.-G., He, F., Wang, C., Zhang, W., Wang, J., 2008. Oil filling history of the Ordovician oil reservoir in the major part of the Tahe oilfield, Tarim Basin, NW China. Organic Geochemistry 39, 1637–1646.
Yu, S., Pan, C., Wang, J., Jin, X., Jiang, L., Liu, D., Lü, X., Qin, J., Qian, Y., Ding, Y., Chen, H., 2011. Molecular correlation of crude oils and oil components from reservoir rocks in the Tazhong and Tabei uplifts of the Tarim Basin, China. Organic Geochemistry 42, 1241–1262.
Yu, S., Pan, C., Wang, J., Jin, X., Jiang, L., Liu, D., Lü, X., Qin, J., Qian, Y., Ding, Y., Chen, H., 2012. Correlation of crude oils and oil components from reservoirs and source rocks using carbon isotopic compositions of individual n-alkanes in the Tazhong and Tabei Uplift of the Tarim Basin, China. Organic Geochemistry 52, 67–80.
Zhan, Z.-W., Tian, Y., Zou, Y.-R., Liao, Z., Peng, P.A., 2016a. De-convoluting crude oil mixtures from Palaeozoic reservoirs in the Tabei Uplift, Tarim Basin, China. Organic Geochemistry 97, 78–94.
Zhan, Z.-W., Zou, Y.-R., Shi, J.-T., Sun, J.-N., Peng, P.A., 2016b. Unmixing of mixed oil using chemometrics. Organic Geochemistry 92, 1–15.
Zhang, L., Li, M., Yang, F., 2012. Progress of geochemical research on dibenzofuran and its chemical mechanism as molecular tracer for oil charging pathways. Oil and Gas Geology 33 (4), 633–639 (in Chinese with English abstract).
Zhang, S., Hanson, A.D., Moldowan, J.M., Graham, S.A., Liang, D., Chang, E., Fago, F., 2000. Paleozoic oil-source rock correlations in the Tarim Basin, NW China. Organic Geochemistry 31, 273–286.
Zhang, S., Liang, D., Zhang, B., 2004. Hydrocarbon Generation from Marine Source Rocks of Tarim Basin. Petroleum Industry Press, Beijing (in Chinese with English foreword).
Zhang, S., Huang, H., 2005. Geochemistry of Palaeozoic marine petroleum from the Tarim Basin, NW China: Part 1. Oil family classification. Organic Geochemistry 36, 1204–1214.
Zhang, S., Huang, H., Xiao, Z., Liang, D., 2005. Geochemistry of Palaeozoic marine petroleum from the Tarim Basin, NW China. Part 2: Maturity assessment. Organic Geochemistry 36, 1215–1225.
Zhang, S., Huang, H., Su, J., Zhu, G., Wang, X., Larter, S., 2014. Geochemistry of Paleozoic marine oils from the Tarim Basin, NW China. Part 4: Paleobiodegradation and oil charge mixing. Organic Geochemistry 67, 41–57.
Zhu, G., Zhang, S., Su, J., Zhang, B., Yang, H., Zhu, Y., Gu, L., 2013. Alteration and multi-stage accumulation of oil and gas in the Ordovician of the Tabei Uplift, Tarim Basin, NW China: implications for genetic origin of the diverse hydrocarbons. Marine and Petroleum Geology 46, 234–250.